Materials Today Bio 22 (2023) 100745

Contents lists available at ScienceDirect

Materials Today Bio

journal homepage: www.journals.elsevier.com/materials-today-bio

Tumor-targeted liposomes with platycodin D2 promote apoptosis in colorectal cancer

Euni Cho [a,b,1], Seok-Jun Mun [a,b,1], Minha Jeon [c,1], Hyo Keun Kim [b,d,1], Hwira Baek [c], Yu Seong Ham [b,d], Woo Jin Gil [b,d], Jin Woong Kim [c,**], Chul-Su Yang [b,d,e,*]

[a] Department of Bionano Engineering Technology, Hanyang University, Seoul, 04673, South Korea
[b] Center for Bionano Intelligence Education and Research, Ansan, 15588, South Korea
[c] School of Chemical Engineering, Sungkyunkwan University, Suwon, 16419, South Korea
[d] Department of Molecular and Life Science, Hanyang University, Ansan, 15588, South Korea
[e] Department of Medicinal and Life Science, Hanyang University, Ansan, 15588, South Korea

ARTICLE INFO

Keywords:
Platycosides
Liposomes
Apoptosis
Colorectal cancer
Xenograft

ABSTRACT

Conventional chemotherapy for colorectal cancer (CRC), though efficacious, is discouraging due to its limited targeting capability, lack of selectivity, and chemotherapy-associated side effects. With the advent of nanomedicines, a liposomal delivery system making use of a combination of anticancer phytochemicals is fast gaining popularity as one of the most promising nanoplatforms for CRC treatment. Rising evidence supports phytochemicals such as platycosides for their anticancer potency. To this end, a combination therapy including tumor-targeted liposomes along with phytochemicals might have a greater therapeutic potential against cancer. In this study, we developed acidity-triggered rational membrane (ATRAM) along with conjugated platycodin D2 (PCD2) and liposomes (PCD2-Lipo-ATRAM) as a tumor-targeting therapy. The PCD2-Lipo-ATRAM treatment demonstrated a successful tumor-targeting ability in the CRC xenografts, in which PCD2 not only exerted a potent antitumor effect by inducing apoptotic cell death and but also functioned as a liposome membrane stabilizer. Moreover, PCD2-Lipo-ATRAM suppressed antiapoptotic BCL-2 family proteins, resulting in enhanced cytotoxicity toward CRC cells by inducing intrinsic caspase-9/-3 mediated apoptosis. Thus, our data has shown that tumor-targeting PCD2-based liposomal systems represent a promising strategy for CRC therapy, since they directly target the tumors, unlike other therapies that can miss the target.

1. Introduction

Colorectal cancer (CRC) is a leading cause of cancer-associated mortality. The balance between the rates of cell growth and apoptosis that maintains the intestinal epithelial cell homeostasis is an important factor in the development of CRC, which means that dysregulated apoptosis is an important factor in CRC [1]. B-cell lymphoma-2 (BCL-2) family proteins, known to be the key regulators of intrinsic apoptosis, are overexpressed in CRC lesions [2], thereby hampering the efficacy of various chemotherapeutics. Hence, BCL-2 is valuable target for CRC therapy. The target of the current chemotherapeutics for CRC treatment is the apoptosis pathway, however, their efficacy is frequently hampered by unfavorable pharmacokinetics and limited targeting efficiency, which results in increased incidence of toxic side effects due to frequent drug administration. Novel approaches are required to overcome dysregulated apoptosis signaling and increase the efficacy of CRC treatment [3].

Phytochemicals, which are naturally occurring saponins obtained from plants, are known to be vital resources in the development of anticancer agents due to their properties such as biological activity, minimal side effects, and low cost. Platycosides (PS) are triterpenoid saponins extracted from Platycodi Radix, and are known to exhibit significant anticancer potency in various types of cancers, including breast cancer [4], lung cancer [5], and colon cancer [6]. These bioactive PS have been proven to promote tumor cell death by regulating various apoptosis-related factors [7,8], making them potent apoptosis-inducing

* Corresponding author. 55 Hanyangdaehak-ro, Sangnok-gu, Ansan-si, Gyeonggi-do, 15588, South Korea.
** Corresponding author. 2066 Seobu-ro, Jangan-gu, Suwon-si, Gyeonggi-do, 16419, South Korea.
E-mail addresses: jinwoongkim@skku.edu (J.W. Kim), chulsuyang@hanyang.ac.kr (C.-S. Yang).
[1] These authors contributed equally to this work

https://doi.org/10.1016/j.mtbio.2023.100745
Received 24 March 2023; Received in revised form 28 June 2023; Accepted 24 July 2023
Available online 29 July 2023

anticancer agents. However, due to poor permeability and low stability, the application of PS as antitumor agents is considerably limited. Fortunately, nanocarriers (drug delivery systems), especially liposomes, can serve as platforms for delivery of these phytochemicals [9]. Increasing evidence supports the fact that encapsulation of saponins with liposomes improve their solubility, bioavailability and enhance therapeutic efficacy [10,11]. For nanotherapeutics are to become efficient anticancer agents, these saponin-based liposomes must penetrate the physiological barrier and reach the tumor site. Most current anticancer nanotherapeutics resort to "passive" targeting strategies [12], which depend solely on the enhanced permeability and retention (EPR) effect to reach the tumor site [13]. However, this strategy can be severely limited by tumor complexity and heterogeneity [14]. It has been observed that only a small percentage of these nanotherapeutics are able to penetrate high-EPR xenografted tumors (less than 1% according to a recent meta-analysis study) [15], necessitating active tumor-targeting strategies. One such active targeting strategy involves enhancement of surface functionalization of liposomes by using tumor-targeting ligands, especially peptides, which can help overcome the current limitations of nanocarriers in the treatment of solid tumors. The pH-responsive acidity-triggered rational membrane (ATRAM) peptide, has been proven to successfully deliver liposomes via pH-responsive membrane interaction into cancer cells within the acidic TME (tumor microenvironment) [16]. We have previously demonstrated that ATRAM-conjugated multifunctional GRA8 peptide has successfully targeted the tumor cells *in vitro* and *in vivo* [17].

In this study, we have designed PS-based liposomes based on the versatile properties of PS and its applicability in CRC therapy. The three PS which are commonly used in cancer therapy, platycodin D (PCD), platycodin D2 (PCD2), and polygalacin D (PGD), were optimized in the current study. We hypothesized that the encapsulation of PS with the liposomes (PS-Lipo) could help overcome their disadvantages such as poor stability and limited permeability, by facilitating intracellular uptake, thereby enhancing their inherent antitumor efficacy. Our *in vitro* mechanistic studies revealed that PS-Lipo induces apoptotic tumor cell death through the caspase-9/3 axis, demonstrating that the mechanism of PS-Lipo is dependent on the intrinsic apoptotic pathway. Since platycodin D2-based liposome (PCD2-Lipo) exhibited the strongest antitumor efficacy than other PS-Lipo molecules, we constructed ATRAM-conjugated PCD2-Lipo (PCD2-Lipo-ATRAM) for tumor-targeting therapy. In CRC xenografts (DLD-1 & CT26), PCD2-Lipo-ATRAM successfully inhibited CRC tumor growth by targeting the tumor sites. The pH-responsive PCD2-Lipo-ATRAM appears to be a promising cancer drug delivery platform that combines stability with effective tumor-targeting and triggers apoptosis of cancer cells.

2. Materials and methods

2.1. Materials

Platycodin D (PCD, MW = 1225.34, purity = 98%), Platycodin D2 (PCD2, MW = 1387.48, purity = 97%), Polygalacin D (PGD, MW = 1209.34, purity = 98%) were purchased from Biopurify Phytochemicals Ltd (China). ATRAM peptide (GLAGLAGLLGLEGLLGLPLGLLEGLWLGLELEGN) was purchased from PEPTRON (Korea). Dulbecco's modified Eagle's medium (DMEM) with High Glucose with L-Glutamine, RPMI-1640 Media with L-glutamine, fetal bovine serum (FBS), streptomycin, penicillin and 0.25% trypsin-EDTA were purchased from GenDEPOT (USA). Quanti-LDH™ PLUS Cytotoxicity Assay Kit (Colorimetric) and Quanti-Max™ WST-8 Cell Viability Assay Kit were purchased from BIOMAX (Republic of Korea). MMR SPARK® microplate reader was purchased from TECAN (Switzerland). Phosphatidylcholine was supplied by Solus Advanced Materials (Korea). Anhydrous methylene chloride, pyridine, N,N-diisopropylethylamine, 4-nitrophenylchloroformate, N-(2-aminoethyl)maleimide trifluoroacetate salt, and IR-783 were purchased from Sigma-Aldrich (USA), and MEL was supplied by DK Bio (Korea). PEO-b-PCL-b-PEO (MW ~20 000 g mol^{-1}, MW of blocks 5000–10000–5000 g mol^{-1}) was kindly supplied by Hyundai Bioland (Korea). Texas Red-DHPE (DHPE; 1,2-dihexadecanoyl-sn-glycero-3-phosphoethanolamine, triethylammonium salt) and 4′,6-diamidino-2-phenylindole (DAPI) was purchased from Thermo Fisher Scientific (USA), and phosphate-buffered saline (PBS) solution was purchased from GIBCO-Thermo Fischer Scientific (USA).

2.2. Cell culture

Primary bone marrow-derived macrophages (BMDMs) were prepared by extracting from female C57BL/6 mice and then differentiated for 5–7 days in media contained with M-CSF. Raw 264.7, DLD-1, CT26, HCT 116, A549, and MB231 cells were purchase by Korean Cell Line Bank (KCLB). BMDMs and Raw 264.7 cells were cultured in DMEM with 10% FBS, streptomycin (100 μg/ml), and penicillin (100U/ml). DLD-1, CT26, HCT116, A549, and MB 231 cells were cultured in RPMI 1640 with 10% FBS, streptomycin (100 μg/ml), and penicillin (100U/ml).

2.3. Animals

Female BALB/c nude mice (6-week-old) were provided by Orient Bio (Republic of Korea) and Wild-type female C57BL/6 mice were provided by Samtako Bio Korea (Republic of Korea), and maintained by standard housing conditions of the Center for Laboratory Animal Science, Hanyang University (Ansan, Republic of Korea). All the animal breeding and experiments were held in accordance with guidelines approved by the IACUC, Hanyang University (protocol 2021-0124, 2021-0271).

2.4. Fabrication and characterization of PS-Lipo

We fabricated 0.5 wt% of liposomes by using three kinds of platycosides (PS): PCD-loaded liposome (PCD-Lipo), PCD2-loaded liposome (PCD2-Lipo), and PGD-loaded liposome (PGD-Lipo). For this, we dissolved phosphatidyl choline and PEO-b-PCL-b-PEO in chloroform and platycosides in methanol, and then mixed the two solutions together in a round-bottomed flask. The mixing ratio of phosphatidylcholine and PEO-b-PCL-b-PEO was adjusted to 9:1 and the concentration of PS was set to 200 μM. For the peptide conjugation, the MEL-maleimide (0.23 mg mL^{-1}), synthesized by following our previous method [18,19], was added to the mixture of amphiphiles. Subsequently, the solvent was evaporated using a rotary evaporator at 40 °C for 1 h to form a thin film on the bottom of round-bottomed flask. Then PBS was added to the flask, and the film was hydrated in a sonicator at 45 °C for 100 min. To determine the encapsulated rate of PS-Lipos, fluorescein isothiocyanate (FITC) was equimolarly conjugated on the primary hydroxyl of PS (PS-FITC) through condensation reaction in methanol for over 6 h. The mixture, packed in a dialysis tube (MWCO: 1000 Da, Fisher Scientific, USA), was dialyzed in double distilled water until no fluorescence is detected in the external medium to avoid the unconjugated FITC. Dialyzed PS-FITC was lyophilized to obtain a bright yellow solid. The PS-FITC was then encapsulated in liposome with the same concentration as PS. Then the encapsulation rate of PS-FITC was measured by using the protamine aggregation method [20,21]. Protamine sulfate was added to the PS-FITC-Lipo solution at a concentration of 5 mg/ml while stirring at 25 °C for 30 min to induce aggregation of liposomes and protamine sulfate. The mixture was then centrifuged for 10 000 rpm at 4 °C, and the pellet was resuspended in methanol. The fluorescence intensities of resuspended pellets and PS-FITC standards were measured with microplate readers in the range of 485 nm–535 nm. Finally, the encapsulation efficiency (EE) was calculated by following equation: EE = (PS-FITC in PS-Lipo/total PS-FITC) × 100 (%).

To conjugate the ATRAM peptide with the MEL-malemide linker co-assembled with the vesicular membrane, ATRAM-cysteamide was added to the liposome dispersion, and mixture was stirred at 4 °C for overnight. The hydrodynamic particle size of PS-Lipo and C-Lipo were measured by

dynamic light scattering (DLS 1070, Malvern, United Kingdom) at 25 °C. The morphology of PS-Lipo and C-Lipo was observed by using a transmission electron microscope (JEM 1010, JEOL, Japan). The drug release of PCD2-Lipo-ATRAM in physiological (pH 7.4) and tumor microenvironment (pH 6.5) conditions was determined using the dialysis method. PCD2-FITC was used for detecting PCD2 in the release medium. PCD2-FITC-Lipo-ATRAM was packed in a dialysis tube (MWCO: 3500 Da, Fisher Scientific, USA) and dialyzed in release medium of different pH (pH 7.4 and pH 6.5 PBS with 5% v/v Tween-80). 1 mL of release medium was collected at a set time interval and replaced with a preheated release medium. The fluorescence intensity of collected medium was measured by microplate reader in the range of 485 nm–535 nm.

2.5. Cellular uptake of PS-Lipo

To observe cellular uptake behavior *in vitro* of PS-Lipo, BMDMs, Raw 264.7, DLD-1, and CT26 cells were dispensed at a density of 5×10^3 cells per well in each 96-well plate (SPL, Korea), incubated and maintained at 37 °C and 5% CO_2 for 24hs. Then, the cells were treated by 5 μM of C-Lipo, PCD-Lipo, PCD2-Lipo and PGD-Lipo with Texas red dye. After the designated time, discard the sample solution, washing was performed twice with sterilized PBS, and fluorescence intensity was measured in the range of 535 nm–595 nm fluorescence using a colorimetric microplate reader.

2.6. Confocal microscopy

In order to observe cellular uptake behavior *in vitro* of PS-Lipo, DLD-1 and CT26 cells were dispensed into each 12-well plate (SPL, Korea) with cover slide, at a density of 2×10^4 cells per well and maintained in incubated at 37 °C and 5% CO_2 conditions. Both cells were treated with PS-Lipo and C-Lipo with Texas Red dye (5 μM in serum-free RPMI-1640) for 1 h. Subsequently, cover slides were washed third time with sterile PBS and fixed with 4% paraformaldehyde. After staining nuclei of cells with DAPI for 10 min, the cells were observed to use a confocal microscopy (LSM 800; Carl Zeiss, Germany).

2.7. In vitro cell viability and cytotoxicity study

BMDMs, Raw 264.7, DLD-1, CT26, HCT 116, A549 and MB231 cells were seeded in 96-well plates (SPL, Korea) at a density of 1×10^4 cells per well and cultured in complete DMEM and RPMI-1640 for 18 h. Then, the cells were treated by a series of concentrations of free-PCD, free-PCD2, free-PGD, PCD-Lipo, PCD2-Lipo and PGD-Lipo. After 48 h of incubation, replace the medium with 100 μl of Quanti-Max solution (10% of each media volume). In addition, the supernatant of cell culture is treated with 10 μl of Quanti-LDH reaction mixture. After 2 h of incubation with 37 °C and 5% CO2, the absorbance of the plates treated with Quanti-Max solution are measured at 450 nm using a colorimetric microplate reader. And after 30 min of incubation with 37 °C and 5% CO2, the absorbance of the plates treated with Quanti-LDH reaction mixture are measured at 490 nm using a colorimetric microplate reader. Cell viability was calculated using untreated cell as a control, and cell cytotoxicity was calculated using dead cells using cell lysis solution as a control.

2.8. Immunoblotting

For immunoblotting, cells were lysed by RIPA Cell Lysis Buffer with EDTA (GenDEPOT, USA) and a protease inhibitor cocktail (Xpert Protease Inhibitor Cocktail Solution; GenDEPOT, USA). The lysate of cells was incubated at 4 °C for 30 min, and then centrifuged at 12,000 g for 10 min at 4 °C. The protein was resolved by SDS-PAGE gel electrophoresis and transferred to a polyvinylidene difluoride (PVDF) membrane (GenDEPOT, USA). Anti-BCL-2 (3498S, CST, USA), Anti-BCL-X_L (2764S, CST, USA), Anti-Mcl-1 (5453S, Cell Signaling Technology (CST, USA), Anti-PARP (9532S, CST, USA), Anti-Cleaved PARP (94885S, CST, USA), Anti-Caspase-9 (9508S, CST, USA), Anti-Cleaved Caspase-9 (52873S, CST, USA), Anti-Caspase-3 (9662S, CST, USA), Anti-Cleaved Caspase-3 (9664S, CST, USA), Anti-Caspase-8 (4790S, CST, USA), Anti-GAPDH (sc-32233, SANTA CRUZ BIOTECHNOLOGY, USA) and Anti-β-Actin (sc-47778, SANTA CRUZ BIOTECHNOLOGY, USA) were incubated overnight at 4 °C. Antibody conjugation was visualized by EzWestLumi plus (ATTO, Japan) and detected by a Vilber chemiluminescence analyzer (Fusion solo; Vilber Lourmat, France).

2.9. Generation of knockout cell lines with CRISPR/Cas9

For Genome Editing caspase-9, DLD-1 and CT26 cells were seeded for 24-well plate (SPL, Korea), at a density of 5×10^4 cells per well, and 37 °C and 5% CO_2 conditions were incubated for 24 h gRNA (CRISPR995170_SGM and CRISPR31379_SGM, Invitrogen, USA), Cas9 Protein (TrueCut™ Cas9 Protein v2, Invitrogen, USA), and lipofectamine mixture (Lipofectamine™ CRISPRMAX™, Invitrogen, USA) which targeted caspase-9, were produced and incubated, and incubation was conducted for 2 days at 37 °C and 5% CO_2 conditions. After selection process with genomic cleavage detection assay, knockout of caspase-9 was confirmed by Quantitative PCR and western blot analyses.

2.10. RNA isolation and Quantitative PCR

Total RNAs were isolated from DLD-1 and CT26 cells with using TRIzol™ Reagent (Invitrogen, USA). And then, 100 ng of total RNA was carried out cDNA synthesis using M-MLV cDNA synthesis kit (Enzynomics, Korea). Quantitative RT PCR analyzed by using method of comparative cycle threshold (CT) were performed on QuantStudio 3 Real-Time PCR Instrument (Applied Biosystems, USA). After predenaturation at 95 °C for 10 min, amplifications were followed by 40 cycles at 95 °C for 15 s, 56 °C for 20 s, and 72 °C for 30 s. The human caspase-9 primer pair was 5′-CATTTCATGGTGGAGGTGAAG-3′ and 5′-GGGAACTGCAGGTGGCTG-3′. The human GAPDH primer pair was 5′-GGTGTGAACCATGAGAAGTATGA-3′ and 5′-GAGTC CTTCCACGATA CCAAAG-3′. The mouse caspase-9 primer pair was 5′-AGTTCCCGGGTGCTGTCTAT-3′ and 5′-GCCATGGTCTTTCTGCTCAC-3′. The mouse GAPDH primer pair was 5′-ACTCCACTCACGGCAA ATTC-3′ and 5′-TCTCCATGGTGGTGAAGACA-3′.

2.11. Preparation of the xenograft mice models

BALB/c nude female mice were used for the tumor xenograft experiments. To assess colorectal tumor-bearing mice, CT26 cells (1×10^6 cells/100 μl/head, n = 5), CT26 caspase-9 K.O cells (1×10^6 cells/100 μl/head, n = 5), DLD-1 cells (3×10^6 cells/100 μl/head, n = 10) and DLD-1 caspase-9 K.O cells (3×10^6 cells/100 μl/head, n = 10) were performed subcutaneous injection into the right axillary region of athymic nude [22]. Animals were observed for 28 days with a tumor volume measurement. The treatment was initiated when the tumor size reached an average volume of 50 or 200 mm^3. The tumor volume was measured every day with skin calipers and calculated as the tumor length × tumor width^2 × 0.5, and represented in mm^3. All animals were maintained in a specific pathogen-free environment [17].

2.12. 12. Histology and immunohistochemistry of tumor tissues

Tumor tissues were fixed in neutral-buffered formalin (pH 7.4) and embedded in paraffin. Tissue slides (4 μm) were stained with hematoxylin and eosin (H&E) and immunohistochemical analyses were performed using the streptavidin-biotin and peroxidase protocol according to the manufacturer's structure (Dako, Carpinteria, CA, USA) to detect Ki-67 (ab16667, ABCAM, USA) and proliferating cell nuclear antigen (PCNA, E-AB-32521, Elabscience, USA) proteins. Immunostaining content were semi-quantified using an image analysis software (Image Pro

Plus 4.5; Media Cybernetics, Bethesda, MD, USA). Brown staining appeared under the optical microscope reflecting the positive antigens, in which a board-certified pathologist (Dr. Min-Kyung Kim, Kim Min-Kyung Pathology Clinic, Seoul, Korea) independently scored each slide without prior knowledge of the therapy groups.

2.13. In vivo biodistribution of PCD2-Lipo in the xenograft mice models

In vivo biodistribution of PCD2-Lipo and PCD2-Lipo-ATRAM with IR783 in the xenograft mouse models established using the DLD-1 cell was observed via the IVIS Spectrum-CT *in vivo* imaging system (PerkinElmer, USA). PCD2-Lipo and PCD2-Lipo-ATRAM (2.5 mg kg^{-1}, 100 μl) was injected intraperitoneally into the tumor-bearing mouse models (n = 3 or 4/group). After the injection, time-dependent whole body NIRF imaging was performed up to 48 h post-injection [22].

2.14. Statistical analysis

All data are reported as mean ± SD or SEM and were analyzed using the Student's *t*-test with a Bonferroni adjustment or ANOVA for multiple comparisons. The statistical software program SPSS (Version 12.0) was used to conduct the analyses (SPSS, Chicago, IL, USA). At $p < 0.05$, differences were judged to be significant. Data for survival were graphed and analyzed using the Kaplan–Meier product limit method, with the log-rank (Man-tele-Cox) test for comparisons in GraphPad Prism (version 5.0, La Jolla, CA, USA). IC_{50} values was calculated by online

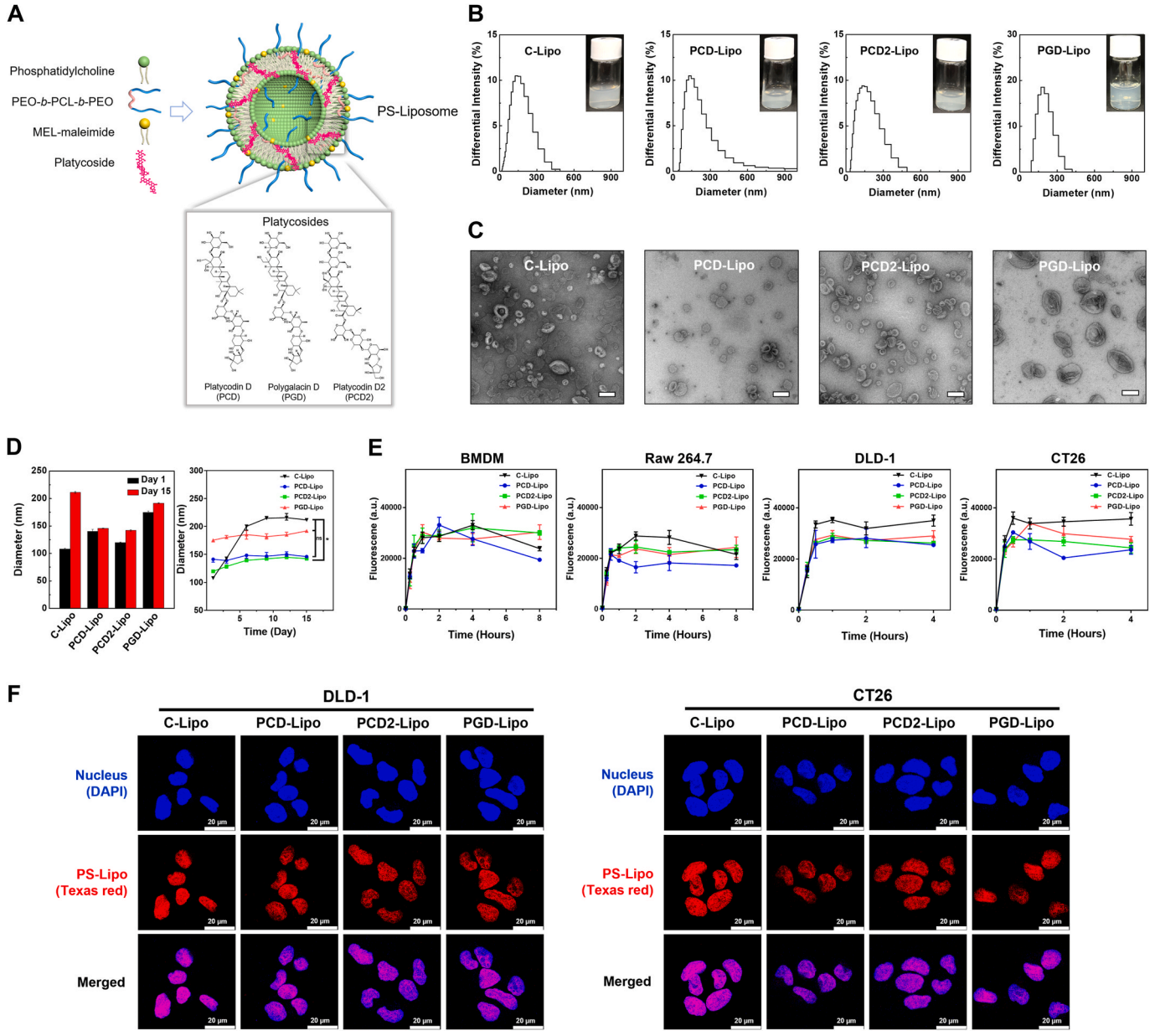

Fig. 1. Preparation and characterization of PS-Lipo. (A) Schematic diagram of platycoside contained liposomes (PS-Lipo) for induction of cancer cell cytotoxicity. (B) Hydrodynamic particle size of C-Lipo, PCD-Lipo, PCD2-Lipo and PGD-Lipo. (C) TEM image of C-Lipo, PCD-Lipo, PCD2-Lipo and PGD-Lipo. Scale bars are 100 nm. (D) Average hydrodynamic particle size of C-Lipo, PCD-Lipo, PCD2-Lipo and PGD-Lipo at Day 1 and Day 15. Means ± SD are shown, significance was measured by paired *t*-test (C-Lipo vs. PCD-Lipo, PCD2-Lipo and PGD-Lipo). *$p < 0.05$. (E) Quantitative analysis of cellular uptake of Texas red–loaded C-Lipo, PCD-Lipo, PCD2-Lipo, or PGD-Lipo by macrophage cells (BMDM and Raw264.7) and cancer cells (DLD-1 and CT26) at 5 μM. (F) Representative confocal laser scanning microscope (CLSM) images of cellular uptake of Texas red–loaded C-Lipo, PCD-Lipo, PCD2-Lipo, or PGD-Lipo by cancer cells (DLD-1 and CT26) after 2 h. Scale bars, 20 μm. (For interpretation of the references to colour in this figure legend, the reader is referred to the Web version of this article.)

tool: MLA "Quest Graph™ IC50 Calculator." AAT Bioquest, Inc., 10 May. 2023, (https://www.aatbio.com/tools/ic50-calculator).

3. Result

3.1. Preparation and characterization of PS-Lipo

In order to overcome the disadvantages of limited delivery efficiency and poor physicochemical properties of PS, we fabricated three different PS-Liposomes (PS-Lipo), namely PCD-Lipo, PCD2-Lipo, and PGD-Lipo (Fig. 1A). We laterally assembled an amphiphilic triblock copolymer, poly(ethylene oxide)-*b*-poly(ε-caprolactone)-*b*-poly-(ethylene oxide) (PEO-*b*-PCL-*b*-PEO), along with the lipid bilayer of liposomes to induce the PEGylation, thus enhancing the membrane modulus and systemic circulation time of liposomes [23]. Moreover, liposomes were prepared by the thin-film hydration method, in order to achieve high encapsulation efficiency and fine particle size distribution of liposomes [24]. The typical vesicular structure of the control liposomes (C-Lipo) and PS-Lipo were verified by transmission electron microscopy (TEM) (Fig. 1B). The average hydrodynamic particle size of the C-Lipo was 108.7 nm with a polydispersity index (PDI) of approximately 0.28. All PS-Lipo molecules had a slightly higher average hydrodynamic particle size as compared to the C-Lipo. The hydrodynamic sizes of PCD-Lipo, PCD2-Lipo, and PGD-Lipo were 139.9 nm, 120.0 nm, and 175.2 nm with the PDI values of 0.350, 0.357, and 0.159, respectively (Fig. 1C). Negligible changes were observed in the particle sizes of the three PS-Lipo formulations, when subjected to long-term stability tests (Fig. 1D). These results suggest that PS was physically and stably immobilized on the lipid bilayers in the liposome systems and did not affect the liposome formation process and long-term storage [25]. We measured the encapsulation efficiency of PS in PS-Lipo by conjugating FITC on the primary hydroxyl group of PS. The encapsulation efficiency of PCD-FITC and PGD-FITC in PS-Lipo was determined above 80%, but that of PCD2-FITC was observed about 62%, probably because the additional glucose chain of PCD2 rather increased the hydrophilicity (Supplementary Fig. 1). In order to determine the uptake efficiency of the prepared PS-Lipo molecules, Texas Red-DHPE-tagged PS-Lipo were treated in macrophage cells (BMDM and Raw 264.7) and cancer cells (DLD-1 and CT26) in a time-dependent manner. All three PS-Lipo molecules exhibited strong red fluorescence signals inside different cells (Fig. 1E & F), suggesting that PS encapsulated by liposomes could be successfully internalized by cells.

3.2. Encapsulating PS with liposomes enhanced cytotoxicity against CRC cells

We examined the antitumor activity of PS-Lipo samples, by subjecting them to WST-8 cell viability and Quanti-LDH (lactate dehydrogenase)™ cytotoxicity assays. Different cancer cells were used in this assay and macrophages were used as controls. First, we tested the viability of macrophages by treating them with free PS and PS-Lipo. As shown in Fig. 2A & B, free PCD, PCD2, and PGD were observed to significantly inhibit the proliferation of macrophages, most likely due to the instability of free platycosides *in vitro*. However, when free PS was encapsulated in liposomes (PS-Lipo), their toxicity to normal cells were substantially reduced, probably because of the increased stability and enhancement of the cellular uptake of free platycosides, indicating that the prepared PS-Lipo molecules possess remarkable biocompatibility at the cellular level. Next, we performed cytotoxicity assays against different cancer cell lines to evaluate the antitumor efficacy of PS-Lipo. The viability of cancer cells from the colon, breast, and lungs was gradually inhibited by each PS-Lipo in a concentration-dependent manner (Fig. 2C & D & Supplementary Fig. 2). Interestingly, each PS-Lipo exerted significant cytotoxicity on various cancer cell lines, with CRC cells being the most sensitive. Consistent with these viability results, the LDH assay showed that PS-Lipo treatment exhibited the strongest cytotoxicity against CRC cell lines (Fig. 2C). The cytotoxicity of the three PS-Lipo for CRC cells was in the order PCD2-Lipo > PGD-Lipo > PCD-Lipo (Fig. 2C). Most cancer cells tend to upregulate the expression levels of BCL-2 protein family, which serves as a classic hallmark of cancer. Among the antiapoptotic BCL-2 protein family, BCL-X_L has been observed to be strongly upregulated in human CRC specimens and plays a crucial role in determining the chemoresistance of colon cancer stem cells [2,26]. Western blot (WB) analysis was carried out using MCL-1, BCL-X_L, and BCL-2 proteins to examine whether the stronger cytotoxicity of PS-Lipo toward CRC cells is associated with the regulation of the BCL-2 family. WB result showed that expression of all BCL-2 proteins was attenuated upon treatment of PCD2-Lipo in DLD-1 and CT26 cells and BCL-X_L was the most potently inhibited (Fig. 2E). This finding implied that the susceptibility of CRC cells to PS-Lipo might be

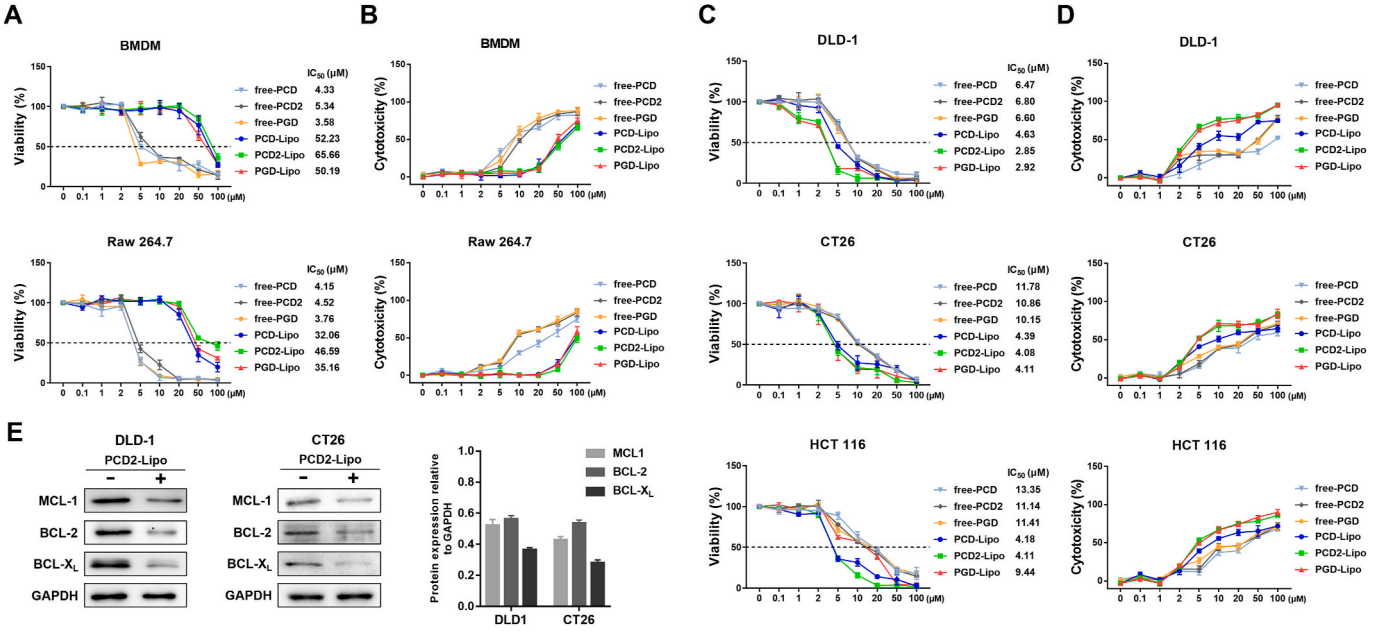

Fig. 2. *In vitro* anticancer activities of platycoside liposomes.

associated with the regulation of the BCL-2 family, especially BCL-X_L. Notably, while free PS was highly cytotoxic to both cancer cells and normal cells, PS-Lipo showed enhanced cytotoxicity against CRC cells, while its toxicity toward normal macrophages was much less. This result demonstrates that liposomal encapsulation of free PS endows it with enhanced antitumor efficacy, particularly toward CRC cells while sparing normal cells.

In vitro cytotoxicity of free PS and PS-Lipo was evaluated for macrophages (A-B) and CRC cells (C-D) by WST-8 cell viability and LDH assay after 48 h of co-incubation. Inset: IC_{50} values (μM) are shown. (E) WB analysis (left) of MCL-1, BCL-2, and BCL-X_L expression in DLD-1 and CT26 cells after treatment of 10 μM and 5 μM PCD2-Lipo for 10 and 8 h and quantification of WB protein levels by group (right).

3.3. PCD2-lipo antitumor efficacy is dependent on the caspase-9/-3 axis

Since PS-Lipo exhibited the highest cytotoxicity against CRC cells (average IC_{50} value of 4.19 μM) as compared to the other cancer cells (average IC_{50} value of 13.31 μM), we selected CRC cells for the following studies. The cytotoxic effect of PS-Lipo on CRC cells can be further explained by alterations in cell death. Platycosides have been reported to exert anticancer activities via apoptotic signaling pathway [27]. As key mediators of apoptosis, caspase-8, caspase-9, and caspase-3 are situated at pivotal junctions in apoptosis pathways (Fig. 3A). The extrinsic pathway is mediated by caspase-8, while the intrinsic pathway can be initiated through caspase-9, and both pathways converge at caspase-3 (the executioner) to finally result in apoptotic cell death [28]. Therefore, we used WB analysis to elucidate the molecular mechanisms of the cytotoxicity and apoptotic effect of PS-Lipo. The expression levels of apoptosis-related proteins (caspase-3, caspase-8, caspase-9, and PARP) were detected in PS-Lipo treated DLD-1 and CT26 cells. As shown in Fig. 3B–E, PS-Lipo increased cleaved caspase-9, cleaved caspase-3 and cleaved PARP expression in a dose-dependent manner, while cleaved caspase-8 showed no alteration in the expression. The results suggest that PS-Lipo exerted cytotoxicity toward CRC cells by inducing caspase-9/-3 dependent apoptosis. To further evaluate whether PS-Lipo-induced apoptosis was dependent with the caspase-9/-3 axis, we generated caspase-9 knockout (KO) DLD-1 and CT26 cells by CRISPR/Cas9-mediated genome editing (Supplementary Figs. 3A and 3B) followed by PCD2-Lipo treatment and assessed cell viability by performing WB analysis. Caspase-9 KO DLD-1 and CT26 cells showed normal growth rates similar to wild-type (WT) DLD-1 and CT26 cells (Supplementary Figs. 3C and 3D). Since the stability, size, and IC_{50} of PCD2-Lipo were more favorable than that of other PS-Lipo molecules

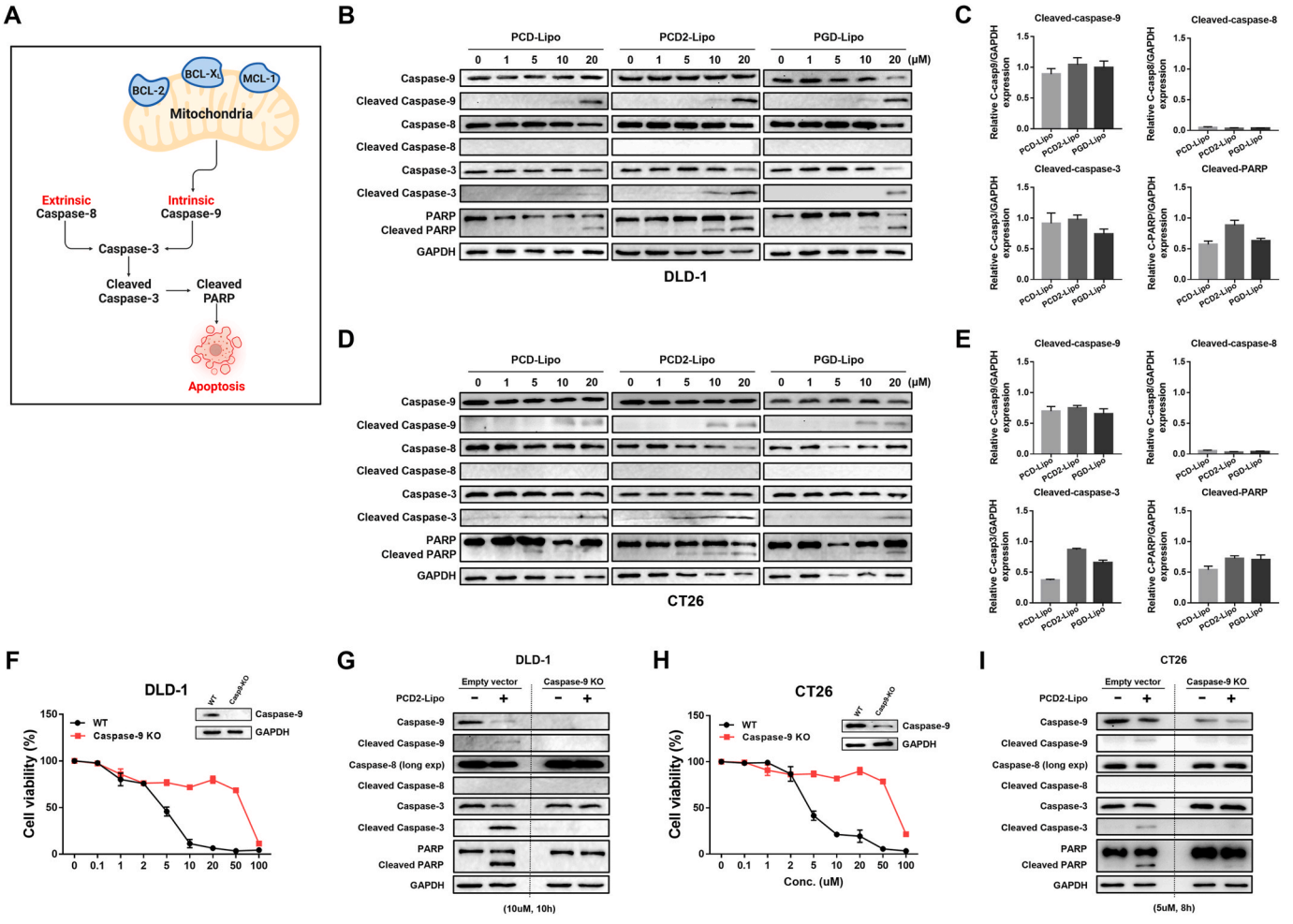

Fig. 3. Inhibition of intrinsic apoptosis (caspase-9) abolished PS-Lipo-induced apoptosis. (A) Schematic representation of the apoptotic pathway. Apoptosis can be induced by either extrinsic pathway through death receptors that specifically activate caspase-8 or intrinsic pathway through expression of BCL2 family BH3-only proteins (BCL-2, BCL-X_L, and MCL-1) that leads to activation of caspase-9. (B & D) WB analysis of caspase-8, caspase-9, caspase-3, PARP, and GAPDH protein expression in DLD-1 cells (B) or CT26 (D) after different PS-Lipo treatments for 8 h (C & E) Quantification of WB protein levels by group in DLD-1 (C) and CT26 (E) cells. (F & H) Cellular cytotoxicity of PCD2-Lipo was evaluated by WST-8 viability assay after 48 h of co-incubation against WT or caspase-9 knockout (KO) DLD-1 cells (F) and CT26 cells (H). (G & I) WB analysis of caspase-8, caspase-9, caspase-3, PARP, and GAPDH protein expression in WT or caspase-9 KO DLD-1 (G) or CT26 cells (I) after different PCD-Lipo treatments for different time.

(Figs. 1 and 2), PCD2-Lipo was selected in this study. After PCD2-Lipo treatment, the cell viability of WT DLD-1 cells was observed to decrease in a dose-dependent manner. However, CRISPR/Cas9 KO of caspase-9 reversed the tumor growth inhibitory effect of PS-Lipo (Fig. 3F & H), indicating that caspase-9 is essentially involved in the growth inhibitory functions of PCD2-Lipo. Under many circumstances, even if a particular caspase is inhibited, apoptosis will still occur by different mechanisms [29]. For example, in the event of the inhibition of the initiator caspase, caspase-9; the executional caspase-3 can still be activated by caspase-8, which is responsible for the extrinsic pathway [30,31]. Considering that PCD2-Lipo cannot exert cytotoxicity against CRC cells under inhibition of caspase-9, our next step was to determine whether the failure of PCD2-Lipo-induced antitumor activity correlated with the inhibition of the caspase-9/-3 axis. Hence, we used WB analysis to evaluate the expression levels of apoptotic factor in the caspase-9 KO conditions through WT cells. Our results demonstrated that the intrinsic apoptotic pathway through the caspase-9/-3 axis is significantly activated in PCD2-Lipo-treated WT DLD-1 and CT26 cells, while this activation of the signaling pathway was abolished in caspase-9 KO DLD-1 (Fig. 3G & I). These findings indicate that, increased levels of caspase-9, caspase-3, and PARP are associated with inhibition of tumor growth, but caspase-8 is not instrumental in this process (Fig. 3G & I). In addition, the expression levels of the caspase-8/-3 axis were not investigated in both WT and caspase-9 KO cells. Collectively, these results demonstrated that the caspase-9/-3-mediated intrinsic pathway specifically responsible for inducing apoptosis in PCD2-Lipo treated DLD-1 cells.

3.4. Tumor-targeting PCD2-Lipo-ATRAM inhibits tumor growth in CRC xenografts

The acidic tumor microenvironment (TME) has been observed to act as biological barriers during *in vivo* drug delivery, which blocks the accumulation of nanotherapeutics at tumor sites [32]. To enhance the *in vivo* tumor-targeting ability, we conjugated PCD2-Lipo to an ATRAM peptide to facilitate internalization of the liposome specifically into tumor cells within the TME. The ATRAM peptide is known to form a transmembraneous helical structure which effectively penetrates the phospholipid bilayer of the cell membrane under acidic conditions [16]. To deposit the ATRAM peptides on the surface of PCD2-Lipo, a mannosylerythritol lipid (MEL)-maleimide linker was synthesized by modifying hydroxy group of MEL to maleimide group [18]. The MEL-maleimide linker is able to directly co-assemble with the lipid layer of liposomes. More specifically, the di-alkyl chain of the MEL-maleimide exists in the hydrophobic region of the lipid bilayer and the hydrophilic maleimide head group is exposed to the aqueous phase. This enables the thiol-ended ATRAM peptide to conjugate with the PCD2-Lipo (PCD2-Lipo-ATRAM) via the thiol-maleimide reaction (Fig. 4A). The hydrodynamic particle size of PCD2-Lipo-ATRAM was measured and was found to be 128.5 nm and had a PDI value of 0.353, which was not significantly different from that of PCD2-Lipo, implying that the conjugation of ATRAM peptide does not affect the physical characteristics of PCD2-Lipo. We also confirmed the vesicular structure of PCD2-Lipo-ATRAM in both physiological condition and acidic condition through TEM observations (Fig. 4B & Supplementary Fig. 4). The structure of PCD2-Lipo-ATRAM on both pH conditions showed no significant difference. Further, the releasing rate of encapsulated PCD2 of PCD2-Lipo-ATRAM under acidic pH conditions was similar to that of physiological pH conditions (Supplementary Fig. 5). To investigate the *in vivo* tumor-targeting ability of the functionalized PCD2-Lipo-ATRAM, we performed near-infrared (NIR) fluorescence imaging using an DLD-1 xenograft model (Fig. 4C). We labeled PCD2-Lipo-ATRAM with IR-783, an NIR lipid dye, (PCD2-Lipo-ATRAM/IR783) and intraperitoneal injected it into DLD-1 tumor–bearing nude mice. PBS and PCD2-Lipo were used as the controls. We performed *in vivo* and *ex vivo* NIR imaging at different time points after injection, using IVIS Lumina II. After individual IR783-labeled liposomes were injected, the PCD2-Lipo-ATRAM group showed a much stronger fluorescence signal in the tumor region at all-time points (Fig. 4D–F), compared with control liposomes, indicating that the accumulation of PCD2-Lipo in the tumor region was significantly enhanced by surface functionalization of the liposomes through ATRAM peptide. PCD2-Lipo without ATRAM peptide showed almost no fluorescence signal. This result clearly demonstrated the tumor-targeting effect of PCD2-Lipo-ATRAM *in vivo*.

We examined the antitumor efficacy of PCD2-Lipo-ATRAM in a xenograft model of DLD-1 and CT26 cells. Having established that the caspase-9/-3 axis play crucial role in PCD2-Lipo-induced apoptosis in DLD-1 and CT26 cells *in vitro* (Fig. 3), we implanted DLD-1 parental (WT) or caspase-9 KO clones (negative controls) subcutaneously into the flanks of nude mice (Fig. 4G). After the tumors reached about 50–150 mm^3, the xenografts received treatment of vehicle, PCD2-Lipo, or PCD2-Lipo-ATRAM, respectively, at a dosage of 2.5 mg kg^{-1} via intraperitoneal injection. As shown in Fig. 4H & I, after a 28-day treatment regimen, PCD2-Lipo-ATRAM exhibited significant growth inhibitory effect on WT DLD-1 and CT26 tumors despite variations in cell growth rates between DLD-1 and CT26 (Supplementary Fig. 6) [33], whereas had no (or very little) effect on caspase-9 KO tumors that exhibited a tumor growth rate comparable to that of WT tumors in vehicle-treated mice. Furthermore, consistent to our observation with biodistribution studies, PCD2-Lipo without ATRAM peptide failed to have a significant effect on WT tumor growth, suggesting that surface functionalization of the liposome by ATRAM peptide significantly increased the *in vivo* antitumor efficacy of PCD2-Lipo.

To confirm that PCD2-Lipo-ATRAM efficacy is dependent on the caspase-9/-3 pathway, we performed both WB and immunohistochemistry analysis with control or caspase-9 KO mice-derived tumor tissue. The WB analysis demonstrated that intrinsic caspase-9/-3 axis-induced apoptosis but the extrinsic caspase-8/-3 axis was not correlated with the reduction of the tumor growth (Fig. 4J), which was further verified by the detection of caspase-9, caspase-3, and PARP cleavage with H&E staining (Fig. 4K). Collectively, our data clearly demonstrated that PCD2-Lipo-ATRAM successfully targeted the tumor site, and thereby exerted a potent antitumor effect in CRC xenograft and that the mechanism of this antitumor effect was dependent on the intrinsic caspase-9/-3 axis.

4. Discussion

It is desirable to design a tumor-targeted delivery system that does not only selectively target acidic TME, but also promotes tumor apoptosis, eventually destroying tumor cells while sparing normal cells. Recently, combined application of bioactive natural platycosides and nanoscience have successfully created safe, biodegradable, and biocompatible drug delivery systems for targeted and efficacious antitumor therapies. In this study, we developed a new tumor-targeted liposomal delivery system based on the versatile properties of platycoside PCD2 for CRC therapy. To achieve tumor-targeting ability, the shell of PCD2-Lipo was functionalized with ATRAM peptide to promote internalization specifically into cancer cells within the acidic TME. PCD2-Lipo-ATRAM successfully reached the tumor site by targeting acidic TME and also exhibited potent proapoptotic activity toward CRC cells.

Emerging evidence suggests that anticancer phytochemicals benefit from reduced toxicity and improved tumor uptake when encapsulated in liposomes [34]. Poor physicochemical properties and stability along with poor solubility limited the use of platycoside PCD2 as a potent therapeutic agent against CRC. In the present study, we found that PCD2 itself did exhibit cytotoxicity toward both CRC and normal cells. However, when PCD2 was encapsulated in a liposome, its effect on tumor cell cytotoxicity and proapoptotic activity was greatly enhanced *in vitro*, while sparing normal cells. Interestingly, PCD2-Lipo showed a more potent cytotoxicity against CRC cells than other cancer types *in vitro*.

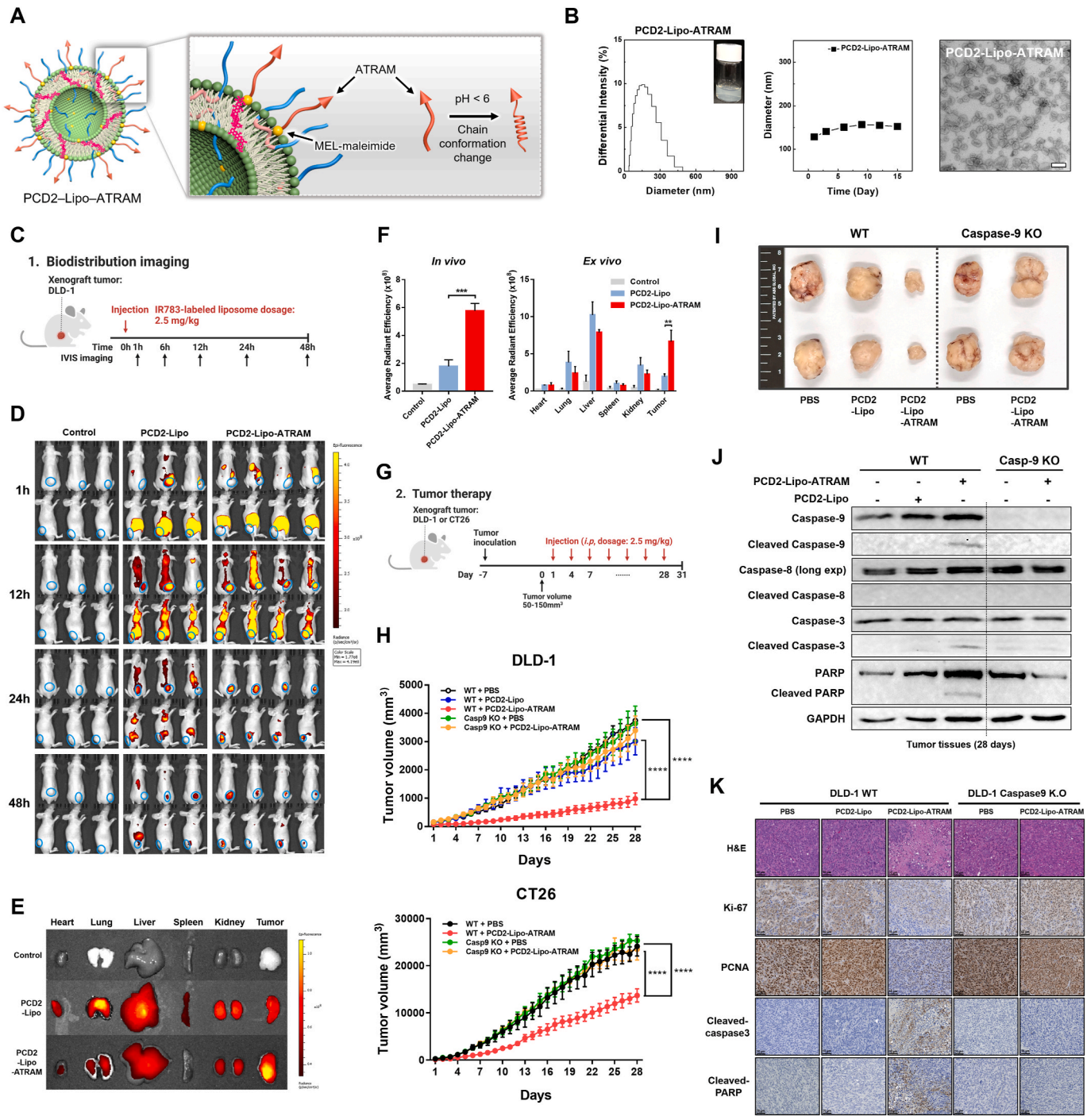

Fig. 4. Tumor-targeting PCD2-Lipo-ATRAM inhibits xenograft CRC tumor growth (A) Schematic Illustration of PCD2-Lipo-ATRAM for targeting acidic tumor microenvironment by pH responsible membrane interaction. Preparation and characterizations of tumor targeting PCD2-Lipo-ATRAM. (B) Characterization of PCD2-Lipo-ATRAM. (C) Schematic design of biodistribution imaging in DLD-1 xenograft model. (D) *In vivo* NIR fluorescent images of nude mice at 1, 12, 24, and 48 h after the administration of PBS, PCD2-Lipo, and PCD2-Lipo-ATRAM; $n = 3$ or 4 per group. (E) Representative *ex vivo* NIR fluorescent images of organs (heart, lung, liver, spleen, and kidney) and excised tumors. (F) *In vivo* & *ex vivo* average radiant efficiency of NIR fluorescent images. *In vivo* NIR fluorescent average radiant efficiency of tumor (24 h after the administration). Means ± SD are shown, significance was measured by unpaired *t*-test (PCD2-Lipo vs. PCD2-Lipo-ATRAM). ***$p < 0.001$. *Ex vivo* NIR fluorescent average radiant efficiency of tissue (heart, lung, liver, spleen, kidney and tumor after 24 h of the administration). Means ± SD are shown, significance was measured by unpaired *t*-test (Tumor PCD2-Lipo vs. Tumor PCD2-Lipo-ATRAM). **$p < 0.05$. (G) Schematic design of tumor therapy in CRC xenografts (DLD-1 or CT26). PBS (control), PCD2-Lipo, or PCD2-Lipo-ATRAM were intraperitoneal administered to wild-type (WT) or Caspase-9 knockout (KO) nude mice after the tumor establishment (50–150 mm^3). (H) Tumor progression was closely monitored by weekly tumor volume measurement using caliper under a 28-day treatment regimen ($n = 5$ to 10 per group). Means ± SEM are shown, significance was measured by two-way ANOVA (WT + PCD2-Lipo-ATRAM vs. WT + PCD2-Lipo and WT + PCD2-Lipo-ATRAM vs. Casp9 KO + PCD2-Lipo-ATRAM). **** denotes $p < 0.0001$. (I) Image of excised xenografted CRC tumors in the five groups at end point (day 28). (J) WB analysis of caspase-9, caspase-8, caspase-3, PARP, and GAPDH protein expression in the five groups. (K) Immunohistochemical staining of tumor sections for hematoxylin and eosin (H&E), cell proliferation marker (Ki-67 and PCNA) and apoptosis marker (cleaved caspase-3 and cleaved PARP). Images were taken at 20 × magnification. Scale bar, 50 μm.

Based on the WB analysis results, it was observed that the potent cytotoxic effect of PCD2 on CRC could be attributed to the inhibition of antiapoptotic BCL-2 family proteins. Resistance to apoptosis by the upregulation of BCL-2 family proteins has been commonly observed in several tumor types [35,36]. Recently, several studies have reported the upregulation of BCL-X_L in colorectal lesions. It has also been observed that targeting BCL-X_L with the highly specific BCL-X_L antagonist A-1155463 considerably impaired the clonogenic potential of adenoma and tumor organoids [26]. These results suggest that CRC tumors seem to depend on BCL-X_L overexpression as strategies for apoptosis evasion [37,38]. The inhibition of BCL-2 family proteins, particularly BCL-X_L, by PCD2 is responsible for the apoptosis of CRC cells, which is beneficial for CRC therapy. Therefore, PCD2 has the potential of a CRC therapeutic agent.

Drug resistance is a common issue in anticancer therapy. Because of the molecular complexities of the tumor microenvironment, single-drug chemotherapy often triggers and reinforces alternative molecular pathways in cancer cells, resulting in drug-resistant mutations. Nowadays, combination drug delivery systems which can target multiple pathways of cancer using multiple drugs simultaneously have been extensively investigated. Liposomes have a unique ability to encapsulate hydrophilic agents in their inner aqueous core and hydrophobic drugs within the lamellae, which makes them versatile therapeutic carriers for combination cancer therapies. Many studies have suggested that the combination of saponin and chemotherapy could significantly enhance the chemosensitivity of tumors to clinically used anticancer drugs such as cisplatin, paclitaxel, doxorubicin, and docetaxel [10,11,39,40]. It has been previously reported that a combination of platycodin D and cetuximab exhibited an obvious synergistic effect on KRAS-mutant CRC cells, potently inhibiting tumorigenesis of CRC xenograft models [41]. In the present study, we discovered that PCD2 not only is an anticancer agent but also has the potential of a membrane stabilizer. The liposomal formulation with PCD2 enhances the stability of liposomes, and also benefits the delivery of anticancer drugs by increasing circulation stability and targeting efficiency. Following internalization into CRC cells, PCD2 exerted its inherent proapoptotic activity, suggesting that PCD2-based liposomes have the potential to exert their synergistic antitumor efficacy with commercial anticancer drugs by acting as a chemosensitizers of anticancer drugs to maximize its chemotherapeutic effect. Therefore, PCD2-Lipo-ATRAM can act as a biocompatible chemo-therapeutic drug nanocarrier for combination cancer therapy.

Nontargeting liposomes, as nanomedicine formulations approved for clinical uses, rely on EPR-based accumulation in tumors, which is critically influenced by the size of nanoparticles (100–200 nm) [42]. The size distribution of PCD2-Lipo is 100–110 nm, which seems suitable for achieving the EPR effect in solid tumors. However, though PCD2-Lipo demonstrated an enhanced anticancer activity against CRC cells *in vitro*, they did not exhibit the same efficacy *in vivo*. When administered *in vivo*, they failed to reach the tumor site, which adversely affected their anticancer effect. The result suggests that tumor accumulation on the basis of size-dependent EPR effect may not be sufficient for achieving effective targeting at tumor sites. Thus, to ensure effective *in vivo* functionality, it is crucial to not only consider the size and stability of liposomes, but also modify the targeting strategy considering the complexity of tumor biology. One property of solid tumors that can be exploited as a tumor-targeting strategy for enhancing the therapeutic benefits of nanomedicine is the acidic niche of TMEs, which mainly arises from the highly glycolytic rate of tumor cells [43]. To facilitate specific tumor-targeting, PCD2-Lipo was functionalized with the pH-responsive ATRAM peptide, which can penetrate the lipid membrane under acidic conditions [44]. After pH-dependent insertion, a fraction of these peptides is also taken up by endocytosis, particularly when the peptide is linked to a liposome [45]. Conjugation of pH-responsive ATRAM peptide with PCD2-Lipo showed successful tumor-targeting and accumulation in the CRC xenografts, which maximizes the tumor inhibiting effect of PCD2. This was further verified in *an in vivo* fluorescence imaging study, where a stronger fluorescence signal of IR783–labeled liposomes was observed in the PCD2-Lipo-ATRAM group than that in PCD2-Lipo.

In summary, we developed a PCD2-based liposomal system as a targeted-tumor therapy for CRC. The PCD2-Lipo-ATRAM system demonstrated successful tumor-targeting ability in the CRC xenografts, which maximizes the tumor inhibition effect of PCD2 by initiating (reactivating) tumor apoptosis. PCD2 in conjugation with liposomes functioned not only as a proapoptotic agent but also as a membrane stabilizer. PCD2-based liposomes offer a novel platform for anticancer drug delivery and may lead to a new era of nanocarrier treatments for cancer.

Author contributions

EC, SJM, HKK, YSH, WJG performed molecular and animal experiments and also analyzed data. MJ, HB, and JWK conceived and designed the PS-Lipo system. MJ and HB fabricated and characterized PS-Lipo. CSY designed and conceptualized the research, supervised the experimental work, analyzed data, and wrote the manuscript.

Statement of significance

Rising evidence supports phytochemicals such as platycosides for their anticancer potency. To this end, a combination therapy including tumor-targeted liposomes along with phytochemicals might have a greater therapeutic potential against cancer. In this study, we developed acidity-triggered rational membrane (ATRAM) along with conjugated platycodin D2 (PCD2) and liposomes (PCD2-lipo-ATRAM) as a tumor-targeting therapy. The PCD2-lipo-ATRAM treatment demonstrated a successful tumor-targeting ability in the CRC xenografts, in which PCD2 not only exerted a potent antitumor effect by inducing apoptotic cell death and but also functioned as a liposome membrane stabilizer. Moreover, PCD2-lipo-ATRAM suppressed antiapoptotic BCL-2 family proteins, resulting in enhanced cytotoxicity toward CRC cells by inducing intrinsic caspase-9/-3 mediated apoptosis. Thus, our data has shown that tumor-targeting PCD2-based liposomal systems represent a promising strategy for CRC therapy, since they directly target the tumors, unlike other therapies that can miss the target.

Declaration of competing interest

The authors declare that they have no known competing financial interests or personal relationships that could have appeared to influence the work reported in this paper.

Data availability

The data that has been used is confidential.

Acknowledgements

This work was supported by the NRF grant funded by the Korea government (MSIP) (2019R1A2C1086383, 2019R1I1A2A01064237 and 2021R1A4A5032463). We would like to thank all members of the Infection Biology Lab for critical reading and discussion of the manuscript.

Appendix A. Supplementary data

Supplementary data to this article can be found online at https://doi.org/10.1016/j.mtbio.2023.100745.

References

[1] P. Ramesh, J.P. Medema, BCL-2 family deregulation in colorectal cancer: potential for BH3 mimetics in therapy, Apoptosis 25 (2020) 305–320.

[2] A.L. Scherr, G. Gdynia, M. Salou, P. Radhakrishnan, K. Duglova, A. Heller, S. Keim, N. Kautz, A. Jassowicz, C. Elssner, Y.W. He, D. Jaeger, M. Heikenwalder, M. Schneider, A. Weber, W. Roth, H. Schulze-Bergkamen, B.C. Koehler, Bcl-xL is an oncogenic driver in colorectal cancer, Cell Death Dis. 7 (2016), e2342.

[3] B. Lim, Y. Greer, S. Lipkowitz, N. Takebe, Novel apoptosis-inducing agents for the treatment of cancer, a new arsenal in the toolbox, Cancers (2019) 11.

[4] S. Zhang, X. Chai, G. Hou, F. Zhao, Q. Meng, Platycodon grandiflorum (Jacq.) A. DC.: a review of phytochemistry, pharmacology, toxicology and traditional use, Phytomedicine 106 (2022), 154422.

[5] T. Li, X. Chen, X. Chen, D.L. Ma, C.H. Leung, J.J. Lu, Platycodin D potentiates proliferation inhibition and apoptosis induction upon AKT inhibition via feedback blockade in non-small cell lung cancer cells, Sci. Rep. 6 (2016), 37997.

[6] C.H. Wang, R. Baskaran, S.S. Ng, T.F. Wang, C.C. Li, T.J. Ho, D.J. Hsieh, C.H. Kuo, M.C. Chen, C.Y. Huang, Platycodin D confers oxaliplatin Resistance in Colorectal Cancer by activating the LATS2/YAP1 axis of the hippo signaling pathway, J. Cancer 14 (2023) 393–402.

[7] M. Khan, A. Maryam, H. Zhang, T. Mehmood, T. Ma, Killing cancer with platycodin D through multiple mechanisms, J. Cell Mol. Med. 20 (2016) 389–402.

[8] A.S. Choudhari, P.C. Mandave, M. Deshpande, P. Ranjekar, O. Prakash, Phytochemicals in cancer treatment: from preclinical studies to clinical practice, Front. Pharmacol. 10 (2019) 1614.

[9] V.P. Chavda, D. Vihol, B. Mehta, D. Shah, M. Patel, L.K. Vora, M. Pereira-Silva, A. C. Paiva-Santos, Phytochemical-loaded liposomes for anticancer therapy: an updated review, Nanomedicine (Lond) 17 (2022) 547–568.

[10] J. Xia, S. Ma, X. Zhu, C. Chen, R. Zhang, Z. Cao, X. Chen, L. Zhang, Y. Zhu, S. Zhang, S. Li, G. Gu, X. Wei, K. Yu, J. Wang, Versatile ginsenoside Rg3 liposomes inhibit tumor metastasis by capturing circulating tumor cells and destroying metastatic niches, Sci. Adv. 8 (2022), eabj1262.

[11] C. Hong, D. Wang, J. Liang, Y. Guo, Y. Zhu, J. Xia, J. Qin, H. Zhan, J. Wang, Novel ginsenoside-based multifunctional liposomal delivery system for combination therapy of gastric cancer, Theranostics 9 (2019) 4437–4449.

[12] D. Rosenblum, N. Joshi, W. Tao, J.M. Karp, D. Peer, Progress and challenges towards targeted delivery of cancer therapeutics, Nat. Commun. 9 (2018) 1410.

[13] D. Peer, J.M. Karp, S. Hong, O.C. Farokhzad, R. Margalit, R. Langer, Nanocarriers as an emerging platform for cancer therapy, Nat. Nanotechnol. 2 (2007) 751–760.

[14] F. Danhier, To exploit the tumor microenvironment: since the EPR effect fails in the clinic, what is the future of nanomedicine? J. Contr. Release 244 (2016) 108–121.

[15] S. Wilhelm, A.J. Tavares, Q. Dai, S. Ohta, J. Audet, H.F. Dvorak, W.C.W. Chan, Analysis of nanoparticle delivery to tumours, Nat. Rev. Mater. 1 (2016), 16014.

[16] V.P. Nguyen, L. Palanikumar, S.J. Kennel, D.S. Alves, Y. Ye, J.S. Wall, M. Magzoub, F.N. Barrera, Mechanistic insights into the pH-dependent membrane peptide ATRAM, J. Contr. Release 298 (2019) 142–153.

[17] J.S. Kim, D. Lee, D. Kim, S.J. Mun, E. Cho, W. Son, C.S. Yang, Toxoplasma gondii GRA8-derived peptide immunotherapy improves tumor targeting of colorectal cancer, Oncotarget 11 (2020) 62–73.

[18] D. Park, J.Y. Lee, H.K. Cho, W.J. Hong, J. Kim, H. Seo, I. Choi, Y. Lee, J. Kim, S. J. Min, S.H. Yoon, J.S. Hwang, K.J. Cho, J.W. Kim, Cell-Penetrating peptide-patchy deformable polymeric nanovehicles with enhanced cellular uptake and transdermal delivery, Biomacromolecules 19 (2018) 2682–2690.

[19] J.Y. Kang, S. Kim, J. Kim, N.G. Kang, C.S. Yang, S.J. Min, J.W. Kim, Cell-penetrating peptide-conjugated lipid/polymer hybrid nanovesicles for endoplasmic reticulum-targeting intracellular delivery, J. Mater. Chem. B 9 (2021) 464–470.

[20] K.K. Gunter, T.E. Gunter, A. Jarkowski, R.N. Rosier, A method of resuspending small vesicles separated from suspension by protamine aggregation and centrifugation, Anal. Biochem. 120 (1982) 113–124.

[21] S.R. Dipali, S.B. Kulkarni, G.V. Betageri, Comparative study of separation of non-encapsulated drug from unilamellar liposomes by various methods, J. Pharm. Pharmacol. 48 (1996) 1112–1115.

[22] S. Jeon, E. Jun, H. Chang, J.Y. Yhee, E.Y. Koh, Y. Kim, J.Y. Jung, E.J. Jeong, J. W. Lee, M.K. Shim, H.Y. Yoon, S. Chang, K. Kim, S.C. Kim, Prediction the clinical EPR effect of nanoparticles in patient-derived xenograft models, J. Contr. Release 351 (2022) 37–49.

[23] J.H. Cho, J.Y. Kang, S. Kim, H.R. Baek, J. Kim, K.S. Jang, J.W. Kim, Skin protein-derived peptide-conjugated vesicular nanocargos for selected skin cell targeting and consequent activation, J. Mater. Chem. B 9 (2021) 4956–4962.

[24] D. Lombardo, M.A. Kiselev, Methods of liposomes preparation: formation and control factors of versatile nanocarriers for biomedical and nanomedicine application, Pharmaceutics 14 (2022).

[25] C. Guo, Y. Su, H. Wang, M. Cao, N. Diao, Z. Liu, D. Chen, M. Kong, A novel saponin liposomes based on the couplet medicines of Platycodon grandiflorum-Glycyrrhiza uralensis for targeting lung cancer, Drug Deliv. 29 (2022) 2743–2750.

[26] S. Colak, C.D. Zimberlin, E. Fessler, L. Hogdal, P.R. Prasetyanti, C.M. Grandela, A. Letai, J.P. Medema, Decreased mitochondrial priming determines chemoresistance of colon cancer stem cells, Cell Death Differ. 21 (2014) 1170–1177.

[27] T. Li, X.H. Xu, Z.H. Tang, Y.F. Wang, C.H. Leung, D.L. Ma, X.P. Chen, Y.T. Wang, Y. Chen, J.J. Lu, Platycodin D induces apoptosis and triggers ERK- and JNK-mediated autophagy in human hepatocellular carcinoma BEL-7402 cells, Acta Pharmacol. Sin. 36 (2015) 1503–1513.

[28] B.A. Carneiro, W.S. El-Deiry, Targeting apoptosis in cancer therapy, Nat. Rev. Clin. Oncol. 17 (2020) 395–417.

[29] A. Boice, L. Bouchier-Hayes, Targeting apoptotic caspases in cancer, Biochim. Biophys. Acta Mol. Cell Res. 1867 (2020), 118688.

[30] S. McComb, P.K. Chan, A. Guinot, H. Hartmannsdottir, S. Jenni, M.P. Dobay, J. P. Bourquin, B.C. Bornhauser, Efficient apoptosis requires feedback amplification of upstream apoptotic signals by effector caspase-3 or -7, Sci. Adv. 5 (2019), eaau9433.

[31] Y. Wu, D. Zhao, J. Zhuang, F. Zhang, C. Xu, Caspase-8 and caspase-9 functioned differently at different stages of the cyclic stretch-induced apoptosis in human periodontal ligament cells, PLoS One 11 (2016), e0168268.

[32] L. Miao, C.M. Lin, L. Huang, Stromal barriers and strategies for the delivery of nanomedicine to desmoplastic tumors, J. Contr. Release 219 (2015) 192–204.

[33] M. Zhu, L. Bai, X. Liu, S. Peng, Y. Xie, H. Bai, H. Yu, X. Wang, P. Yuan, R. Ma, J. Lin, L. Wu, M. Huang, Y. Li, Y. Luo, Silence of a dependence receptor CSF1R in colorectal cancer cells activates tumor-associated macrophages, J Immunother Cancer 10 (2022).

[34] V. Rendo, I. Stoimenov, A. Mateus, E. Sjoberg, R. Svensson, A.L. Gustavsson, L. Johansson, A. Ng, C. O'Brien, M. Giannakis, P. Artursson, P. Nygren, I. Cheong, T. Sjoblom, Exploiting loss of heterozygosity for allele-selective colorectal cancer chemotherapy, Nat. Commun. 11 (2020) 1308.

[35] T. Ni Chonghaile, K.A. Sarosiek, T.T. Vo, J.A. Ryan, A. Tammareddi, G. Moore Vdel, J. Deng, K.C. Anderson, P. Richardson, Y.T. Tai, C.S. Mitsiades, U. A. Matulonis, R. Drapkin, R. Stone, D.J. Deangelo, D.J. McConkey, S.E. Sallan, L. Silverman, M.S. Hirsch, D.R. Carrasco, A. Letai, Pretreatment mitochondrial priming correlates with clinical response to cytotoxic chemotherapy, Science 334 (2011) 1129–1133.

[36] T.T. Vo, J. Ryan, R. Carrasco, D. Neuberg, D.J. Rossi, R.M. Stone, D.J. Deangelo, M. G. Frattini, A. Letai, Relative mitochondrial priming of myeloblasts and normal HSCs determines chemotherapeutic success in AML, Cell 151 (2012) 344–355.

[37] P. Ramesh, T.R.M. Lannagan, R. Jackstadt, L. Atencia Taboada, N. Lansu, P. Wirapati, S.R. van Hooff, D. Dekker, J. Pritchard, A.B. Kirov, S.M. van Neerven, S. Tejpar, G. Kops, O.J. Sansom, J.P. Medema, BCL-XL is crucial for progression through the adenoma-to-carcinoma sequence of colorectal cancer, Cell Death Differ. 28 (2021) 3282–3296.

[38] J.D. Leverson, D.C. Phillips, M.J. Mitten, E.R. Boghaert, D. Diaz, S.K. Tahir, L. D. Belmont, P. Nimmer, Y. Xiao, X.M. Ma, K.N. Lowes, P. Kovar, J. Chen, S. Jin, M. Smith, J. Xue, H. Zhang, A. Oleksijew, T.J. Magoc, K.S. Vaidya, D.H. Albert, J. M. Tarrant, N. La, L. Wang, Z.F. Tao, M.D. Wendt, D. Sampath, S.H. Rosenberg, C. Tse, D.C. Huang, W.J. Fairbrother, S.W. Elmore, A.J. Souers, Exploiting selective BCL-2 family inhibitors to dissect cell survival dependencies and define improved strategies for cancer therapy, Sci. Transl. Med. 7 (2015), 279ra240.

[39] C. Cheon, S.G. Ko, Synergistic effects of natural products in combination with anticancer agents in prostate cancer: a scoping review, Front. Pharmacol. 13 (2022), 963317.

[40] Z. Lu, W. Song, Y. Zhang, C. Wu, M. Zhu, H. Wang, N. Li, Y. Zhou, H. Xu, Combined anti-cancer effects of platycodin D and sorafenib on androgen-independent and PTEN-deficient prostate cancer, Front. Oncol. 11 (2021), 648985.

[41] Y. Liu, S. Tian, B. Yi, Z. Feng, T. Chu, J. Liu, C. Zhang, S. Zhang, Y. Wang, Platycodin D sensitizes KRAS-mutant colorectal cancer cells to cetuximab by inhibiting the PI3K/Akt signaling pathway, Front. Oncol. 12 (2022), 1046143.

[42] K. Maruyama, Intracellular targeting delivery of liposomal drugs to solid tumors based on EPR effects, Adv. Drug Deliv. Rev. 63 (2011) 161–169.

[43] B.B. Mendes, D.P. Sousa, J. Conniot, J. Conde, Nanomedicine-based strategies to target and modulate the tumor microenvironment, Trends Cancer 7 (2021) 847–862.

[44] V.P. Nguyen, D.S. Alves, H.L. Scott, F.L. Davis, F.N. Barrera, A novel soluble peptide with pH-responsive membrane insertion, Biochemistry 54 (2015) 6567–6575.

[45] V.P. Nguyen, A.C. Dixson, F.N. Barrera, The effect of phosphatidylserine on a pH-responsive peptide is defined by its noninserting end, Biophys. J. 117 (2019) 659–667.